Microwave-tunable diode effect in asymmetric SQUIDs with topological Josephson junctions

Joseph J. Cuozzo [1,*] Wei Pan [1] Javad Shabani,[2] and Enrico Rossi [3]

[1]*Materials Physics Department, Sandia National Laboratories, Livermore, California 94551, USA*
[2]*Center for Quantum Information Physics, Department of Physics, New York University, New York, New York 10003, USA*
[3]*Department of Physics, William and Mary, Williamsburg, Virginia 23187, USA*

In superconducting systems in which inversion and time-reversal symmetry are simultaneously broken the critical current for positive and negative current bias can be different. For superconducting systems formed by Josephson junctions (JJs) this effect is termed Josephson diode effect. In this paper, we study the Josephson diode effect for a superconducting quantum interference device (SQUID) formed by a topological JJ with a 4π-periodic current-phase relationship and a topologically trivial JJ. We show how the fractional Josephson effect manifests in the Josephson diode effect with the application of a magnetic field and how tuning properties of the trivial SQUID arm can lead to diode polarity switching. We then investigate the ac response and show that the polarity of the diode effect can be tuned by varying the ac power and discuss differences between the ac diode effect of asymmetric SQUIDs with no topological JJ and SQUIDs in which one JJ is topological.

I. INTRODUCTION

Recently there has been a great deal of activity investigating nonreciprocal effects and supercurrent rectification in superconductors [1–16] and Josephson junctions (JJs) [17–32]. Conventional diodes, such as *p-n* junctions, have electrical resistance that depends on the direction of current and have numerous applications in computing, logic, and detection. The superconducting diode effect is characterized by a difference in forward and reverse critical currents I_+ and I_- where the current range between I_+ and I_- can be used to achieve supercurrent rectification. This nonreciprocal supercurrent develops due to simultaneous breaking of time-reversal and inversion symmetry [29,33–35]. Despite superconducting diodes having been discussed long ago [17,36–40], there has been a revival of interest, in part, due to signatures of finite-momentum Cooper pairing in helical superconductors [8,26,30] associated with the Josephson diode effect (JDE). Superconducting diodes can also be used as passive on-chip gyrators, circulators, and memory in cryogenic applications [41].

The fractional Josephson effect [42,43] describes a 4π-periodic current-phase relationship (CPR) in JJs originally associated with topological superconductivity. Topological superconductivity has made important strides over the past decade since theoretical proposals to create topological superconductors for use in quantum computing have become feasible to realize [44–50], although their discovery is still inconclusive [51–65]. Despite this, the fractional Josephson effect is well documented in both topological [19,66–69] and

trivial JJs [70]. Furthermore, planar JJs are a suitable platform to realize a large JDE since both time-reversal and inversion symmetry can be readily and controllably broken [71,72].

In this paper we study the dc and ac response of asymmetric SQUIDs [73]. Compared to previous studies we take into account effects due to the SQUID's inductance, the presence of an ac bias, and the role that a non-negligible fractional, 4π, component of the CPR for one of the JJ forming SQUIDs has on the SQUID's diode effect. We call a SQUID in which one JJ's CPR is 4π a 2π-4π SQUID. Recent experiments have shown that high-transparency wide JJs can also have a 4π-periodic component of the current-phase relationship [70]. Our approach and results do not depend on the origin of the 4π-periodic component and therefore apply directly also to SQUIDs in which one JJ is wide and very transparent, as the one studied in Ref. [70]. First, we treat the problem with an analytic model that goes beyond the minimal models considered before [72,74,75]. We show that the dc response of 2π-4π SQUIDs exhibits the JDE and that the diode polarity is reversible with asymmetry in the normal resistance of the two SQUID arms. We compare the JDE of a topological SQUID to a topologically trivial one and find that, despite both SQUIDs showing comparable diode efficiencies, topological SQUIDs are of higher practical quality given they have a larger rectification current window ΔI_c coinciding with large diode efficiency making them more robust to, e.g., stray magnetic fields. We also show the JDE can be switched and enhanced by an ac drive allowing for a microwave-controlled diode effect. By including the inductance's effects we are able to properly characterize the ac response of the SQUID and show that the strength and sign of the diode effect depend on the ac power, an additional contribution toward the understanding of the physics of asymmetric SQUIDs. Lastly, we compare our analytic results with numerical simulations of the ac response of trivial asymmetric and 2π-4π SQUIDs and find good agreement between the two approaches.
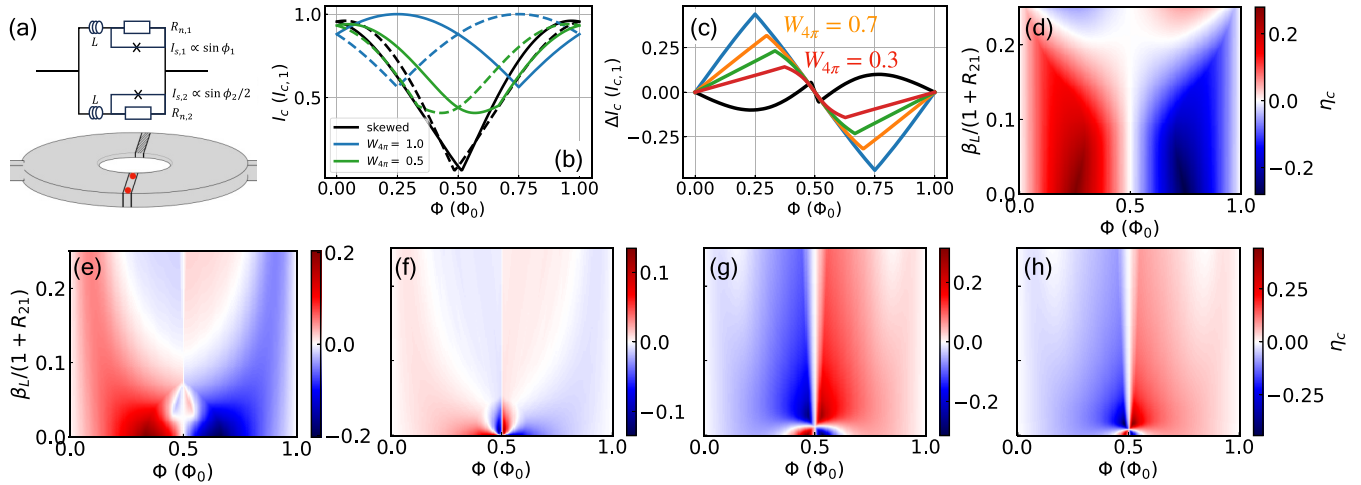
---

*jjcuozz@sandia.gov

FIG. 1. (a) Circuit diagram of a 2π-4π SQUID hosting Majorana zero modes in one arm. (b) SQUID oscillations for I_+ (solid) and I_- (dashed) with $\beta_L = 0$. Skewed SQUID parameters are $a_1 = 1$ and $a_2 = 0.9 = 1 - c_2$ and (c) corresponding critical current difference for an asymmetric SQUID with $a_1 = 1$, $b_2 = W_{4\pi} = 1 - a_2$. η_c dependence on Φ and $\frac{\beta_L}{1+R_{21}}$ for $a_1 = 1$ and (d)$W_{4\pi} = 1$, (e) $W_{4\pi} = 0.5$, (f) $W_{4\pi} = 0.1$, (g) $a_2 = 0.8$, $b_2 = 0.1 = c_2$, and (h) $a_2 = 0.9 = 1 - c_2$ (skewed SQUID).

II. MODEL

To model the dynamics of the JJs we use the resistively shunted junction model, $I_B = \frac{V_J}{R_n} + I_s$, where a current bias I_B across a JJ is split into a resistive channel associated with quasiparticle current with normal resistance R_n and a supercurrent channel I_s. Here we ignore charging effects associated with a capacitive channel. It is known that the Coulomb energy E_C can compete with the Josephson energy E_J in a 2π-4π SQUID and lead to a gap in the midgap spectrum [76] associated with quantum phase slips, reducing the 4π periodicity to 2π. Here we assume $E_J > E_C$ for both SQUID arms, corresponding to wide topological JJs [48,49].

We can describe the fluxoid quantization condition with s-wave superconducting electrodes for the SQUID shown in Fig. 1(a). If the superconducting electrodes are thicker than the London penetration depth and the arms have equal inductance then we have the following current conservation and flux quantization conditions: $I_B = I_1 + I_2$, $\phi_2 - \phi_1 = \frac{2\pi}{\Phi_0} \Phi_{\text{tot}} (\text{mod} 2\pi)$ where $\Phi_{\text{tot}} = L(I_1 - I_2) + \Phi$ and $I_k = \frac{V_{J,k}}{R_{n,k}} + I_{s,k}$, $k = 1, 2$. Here I_1 and I_2 are the currents in each of the SQUID arms, ϕ_1 and ϕ_2 are the gauge-invariant phase differences across each of the SQUID arms, Φ is the total external magnetic flux through the SQUID, L is the inductance associated with the screening flux, Φ_0 denotes the superconducting magnetic flux quantum $h/2e$, and $V_{J,k}$ and $I_{s,k}$ are the potential difference and the supercurrent of the kth arm, respectively. In this paper, we define an asymmetric SQUID as a SQUID with at least one of the following conditions: $I_{s,1}(\phi) \neq I_{s,2}(\phi)$, $I_{c,1} \neq I_{c,2}$, or $R_{n,1} \neq R_{n,2}$. Using the Josephson relation $V_{J,k} = (\hbar/2e)\dot{\phi}_k$, we can combine these equations and solve for two coupled differential equations in terms of the average phase $\phi_A = (\phi_1 + \phi_2)/2$, and phase difference is $\Psi = (\phi_2 - \phi_1)/2\pi$:

$$\frac{d\phi_A}{d\tau} = \frac{1 + R_{21}}{4} i_B - \frac{i_{s,1} + \Delta_{21} i_{s,2}}{2} + \frac{1 - R_{21}}{4\beta_L}(\Psi - \hat{\Phi}), \quad (1)$$

$$\frac{d\Psi}{d\tau} = \frac{R_{21} - 1}{4\pi} i_B + \frac{i_{s,1} - \Delta_{21} i_{s,2}}{2\pi} - \frac{1 + R_{21}}{4\pi\beta_L}(\Psi - \hat{\Phi}), \quad (2)$$

where $\tau = (2\pi I_{c,1} R_{n,1}/\Phi_0)t$ is a dimensionless time, $R_{21} = R_{n,2}/R_{n,1}$, $\Delta_{21} = R_{21}I_{c,2}/I_{c,1}$, $\beta_L = I_{c,1}L/\Phi_0$, $i_{s,k} = I_{s,k}/I_{c,1}$, and $\hat{\Phi} = \Phi/\Phi_0$.

Evidence for nonsinusoidal terms contributing to a skewed CPR have been observed in past experiments [67,69,70,77–79]. To account for the presence of both skewed and topological CPRs, we assume a CPR with π-, 2π-, and 4π-periodic channels:

$$i_{s,1}(\phi_1) = a_1 \sin(\phi_1) + b_1 \sin\left(\frac{\phi_1}{2}\right) + c_1 \sin(2\phi_1), \quad (3)$$

$$\Delta_{21} i_{s,2}(\phi_2) = a_2 \sin(\phi_2) + b_2 \sin\left(\frac{\phi_2}{2}\right) + c_2 \sin(2\phi_2). \quad (4)$$

The 2π-periodic term of the current-phase relationship is standard for a JJ, the 4π-periodic contribution is present either from the topological character of the JJ or from Landau-Zener transitions in high-transparency JJs, and the π-periodic term is the leading term that needs to be included to describe JJs with good transparency. For a ballistic short junction with a mode with transmission τ, the CPR is described by $I_s(\phi) \propto \sin\phi/\sqrt{1 - \tau \sin^2(\phi/2)}$, where $0 \leqslant \tau \leqslant 1$ and ϕ is the phase across the junction. A Fourier expansion of the CPR to the second harmonic gives $I_s(\phi) \approx I_1 \sin(\phi) + I_2 \sin(2\phi)$, where $I_1 > I_2$ and I_2/I_1 depends on τ. For realistic values of τ, we have $I_2/I_1 \lesssim 0.1$. With this in mind, we constrain the amplitude $c_i \leqslant 0.1$ in our calculations. We assume $a_1 + b_1 + c_1 = 1$ and $a_2 + b_2 + c_2 = \Delta_{21}$ throughout the paper for simplicity. Furthermore, we assume $\Delta_{21} = 1$ throughout the paper, which implies the gaps of the junctions in the SQUID are the same. Following previous work [80], we can reduce the SQUID dynamical equations to a single equation of motion by considering β_L, $|1 - R_{21}| \ll 1$. Retaining terms linear in β_L, the SQUID dynamics are determined by the average phase ϕ_A:

$$\frac{d\phi_A}{d\tau} = \frac{i_B}{2} - \tilde{i}_s(\phi_A) + \frac{\pi\beta_L(c_1 - c_2)^2}{2(1 + R_{21})}\sin(4\pi\hat{\Phi}), \quad (5)$$

where

$$\tilde{i}_s(\phi_A) = \sum_{m=1}^{6} \left[x_m \sin\left(m\frac{\phi_A}{2}\right) + y_m \cos\left(m\frac{\phi_A}{2}\right) \right] + x_8 \sin(4\phi_A) + y_8 \cos(4\phi_A), \quad (6)$$

where x_m and y_m are coefficients that depend on $\hat{\Phi}$, a_i, b_i, c_i, and $\beta_L/(1 + R_{21})$ [81]. The diode efficiency $\eta_c \equiv (I_+ - I_-)/(I_+ + I_-)$ is often used to characterize superconducting diodes where the critical current I_+ $(-I_-)$ corresponds to positive (negative) current bias. In an asymmetric SQUID, the broken chiral symmetry is due to different properties in the two arms of the SQUID, and the broken time-reversal symmetry is due to a magnetic flux threading the SQUID ring. For instance, in the topologically trivial asymmetric SQUID in Ref. [74], the diode is only present if an anomalous supercurrent exists at zero phase bias. This anomalous current breaks the chiral symmetry of the SQUID. We extract $I_{\pm}$ from Eq. (5) where the last two terms describe an effective CPR. First, it is worth noting that the effect of screening enters the dynamics via the term $\beta_L/(1 + R_{21})$, suggesting an increase of R_{21} is similar to a decrease of β_L. The presence of R_{21} in the effective CPR of the SQUID can be traced back to SQUID inductance contribution to the total magnetic flux where the currents I_1 and I_2 are currents which include both the supercurrent channels *and* normal channels. Second, the last term in Eq. (5) is independent of ϕ_A but odd in $\hat{\Phi}$. This term applies an overall shift in the CPR which suggests a bipartite form of the diode effect $I_+ - I_- = \Delta\tilde{i}_{s,c} + \frac{\pi\beta_L(c_1-c_2)^2}{2(1+R_{21})}\sin(4\pi\hat{\Phi})$, where the former term $\Delta\tilde{i}_{s,c} = \max(\tilde{i}_s) + \min(\tilde{i}_s)$ is determined by Eq. (6) and the latter is ϕ_A independent and associated with the screening current of imbalanced π channels. In general, a SQUID with asymmetric skewed CPRs can expect additional contributions to the screening current term, and such shifts to the CPR can contribute to anomalous scenarios such as $|\eta_c| > 1$.

III. RESULTS

We start by considering two types of SQUIDs. The first is a 2π-4π SQUID with 4π supercurrent in the topological arm characterized by the parameter $W_{4\pi} = b_2 = 1 - a_2$. The second is a trivial asymmetric SQUID (skewed SQUID) with $a_1 = 1$ and $a_2 = 0.9 = 1 - c_2$ ($b_1 = 0 = b_2$).

The dc responses of the SQUIDs are shown in Fig. 1(b). We notice that I_c is largest when $\Phi = \Phi_0/4$ for the 2π-4π SQUID. To understand this, recall that for a trivial SQUID with sinusoidal CPRs the currents are maximized at $\phi_{\max} = \pi/2$ and the two arms of the SQUID can simultaneously have that phase $\phi_{\max}$ if the magnetic flux is an integer multiple of the magnetic flux quantum. Now, for the 2π-4π SQUID, if the trivial arm has $\phi_{\max,2\pi} = \pi/2$ and the nontrivial arm has $\phi_{\max,4\pi} = \pi$, then it follows from the same argument that the maximum should occur at $\Phi_{\mathrm{ext}} = \Phi_0/4$ [72,82].

In Fig. 1(c), we present the difference in critical currents $\Delta I_c = I_+ - I_-$ for the 2π-4π SQUID and trivial asymmetric SQUID considered in Fig. 1(b). A clear Josephson diode effect develops at $\Phi \neq n\Phi_0/2$ ($n \in \mathbb{Z}$). Note, ΔI_c of the 2π-4π SQUID exceeds that of the trivial asymmetric SQUID until $W_{4\pi} < 0.3$.

We present η_c dependence on Φ and screening $\beta_L/(1 + R_{21})$ for 2π-4π SQUIDs in Figs. 1(d)–1(f). The diode efficiency of the 2π-4π SQUID shown in Fig. 1(d) shows extrema for $\beta_L/(1 + R_{21}) = 0$ and diode polarity switching for large screening. As $W_{4\pi}$ is decreased from unity [Figs. 1(e) and 1(f)], η_c varies but the tunability of the diode polarity persists. Furthermore, as $W_{4\pi}$ decreases, the diode efficiency is generally smaller.

For a SQUID nearly saturated with trivial supercurrent ($a_1 = 1$, $a_2 = 0.8$, and $b_2 = c_2 = 0.1$), the regime of polarity switching with β_L is pushed beyond our approximation of $\beta_L \ll 1$ [Fig. 1(g)] and closely resembles the trivial asymmetric SQUID dc response [Fig. 1(h)]. In the case of a trivial symmetric SQUID where $a_1 = 1 = a_2$, the diode efficiency $\eta_c = 0$ regardless of the value of Φ and R_{21} [74]; this also holds for $\beta_L > 0$. The source of the diode polarity switching with $\beta_L/(1 + R_{21})$ is higher harmonic contributions to the CPR associated with the screening current ($\beta_L > 0$). The inclusion of β_L and R_{21} is one of our main analytic results. We also see that η_c of the trivial asymmetric SQUID can be larger than η_c of the 2π-4π SQUID. The reason for this is that η_c approaches unity when one of the critical currents approaches zero. Typically, this indicates an ideal diode, but if the nonzero critical current is also extremely small the practicality of such a diode is diminished since the current window for supercurrent rectification is also small. Using $|\Delta I_c|$ as an additional quality factor we find that the 2π-4π SQUID diode outperforms the trivial asymmetric SQUID (see Appendix D and Fig. 6). The smallness of I_c at half flux is also the reason for the presence of strong variations and polarity switchings of η_c when $\Phi/\Phi_0 \approx 1/2$. Such variations are physically uninteresting. In the remainder when discussing polarity switchings of η_c we refer to switchings at values of Φ/Φ_0 away from $1/2$. We discuss η_c in the remainder of the paper for simplicity and comparison with the available literature, but we caution against an overemphasis on optimizing η_c without consideration of the operational current range ΔI_c. Our results also suggest the control of the diode polarity with R_{21} could be used as a signature of the fractional Josephson effect.

To study the ac response of asymmetric SQUIDs we first consider the voltage-biased case, since in this regime we can obtain analytical results. Assuming $V(t) = V_{\mathrm{DC}} + V_{\mathrm{AC}}\cos(2\pi f t)$, from the Josephson relation $\hbar d\phi_A/dt = 2eV$, we obtain $\phi_A(t) = \phi_0 + \omega_0 t + z\sin(2\pi f t)$ where ϕ_0 is an arbitrary integration constant, $z = 2eV_{\mathrm{AC}}/(hf)$, and $\omega_0 = 2eV_{\mathrm{DC}}/\hbar$. Using Eqs. (5) and (6) we can obtain the $\bar{I} - V_{\mathrm{DC}}$, with $\bar{I}$ being the time-averaged current, characteristic of the SQUID. In the remainder we focus on the behavior of the current when $V_{\mathrm{DC}} = 0$.

Figures 2(a) and 2(b) show the SQUID critical current $I_{\mathrm{avg}} \equiv I_+ + I_-$ as a function of Φ and V_{AC} for $\beta_L/(1 + R_{21}) = 0$ and 0.125, respectively, for the skewed SQUID. In the absence of screening, I_{avg} has a high degree of symmetry in (Φ, V_{AC}) space defined by lines of $I_{\mathrm{avg}} = 0$ at $\Phi = \Phi_0/2$ and $V_{\mathrm{AC}} \approx 2.5\, hf/2e$. With screening, lines of $I_{\mathrm{avg}} = 0$ become broken and distorted. To see how this translates to the JDE, we present the corresponding diode efficiency in Figs. 2(c) and 2(d). We immediately notice the symmetry of I_{avg} is preserved in η_c, particularly where $I_{\mathrm{avg}} \approx 0$. In fact, η_c has extrema near $I_{\mathrm{avg}} \approx 0$ as a consequence of $I_{\pm} \to 0$ and $I_{\mp} > 0$, as discussed
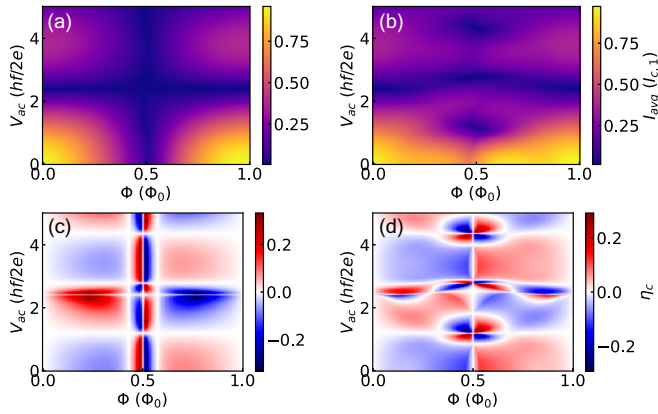
FIG. 2. AC power dependence of I_c and η_c for the skewed SQUID with (a), (c) $\frac{\beta_L}{1+R_{21}} = 0$ and (b), (d) $\frac{\beta_L}{1+R_{21}} = 0.125$.

earlier. We observe periodic diode polarity switching with increasing microwave power V_{AC} for fixed Φ.

We can compare the ac response of the skewed SQUID of Fig. 2 with a 2π-4π SQUID shown in Fig. 3. Figures 3(a) and 3(b) show the ac response for $\beta_L/(1 + R_{21}) = 0$ and 0.125, respectively. We notice the extrema of η_c occur further away from $\Phi = \Phi_0/2$ compared to a trivial asymmetric SQUID, and the magnitude of V_{AC} required to flip the diode polarity is generally larger than that of a trivial SQUID by a factor of 2. The change in diode polarity can be attributed to the $J_0(z/2)$ Bessel function contribution to the gap, associated with the 4π channel, which evolves with z more slowly than the trivial Bessel dependence. Similar to a trivial asymmetric SQUID, a screening current distorts the symmetry of $\eta_c(\Phi, V_{AC})$.

In Fig. 4, we consider the influence of microwave power in the experimentally relevant current bias regime. We numerically solve the coupled system of nonlinear differential equations described in Eq. (2) where we are not limited by the approximation $\beta_L, |1 - R_{21}| \ll 1$ used thus far. We consider a current bias $I_B = I_{DC} + I_{AC}\cos(2\pi ft)$ with a driving frequency $hf/\pi\Delta = 0.6$ where $\pi\Delta \equiv 2eI_cR_n$ [83].
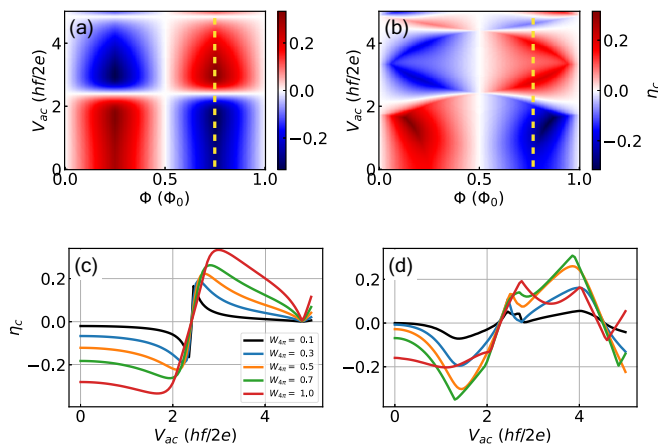

FIG. 3. AC power dependence of η_c for a 2π-4π SQUID with (a)$\beta_L = 0$ and (b)$\beta_L/(1 + R_{21}) = 0.125$. η_c vs V_{AC} at $\hat{\Phi} = 3/4$ for $a_1 = 1$ with (c)$\beta_L = 0$ and (d)$\beta_L/(1 + R_{21}) = 0.125$.
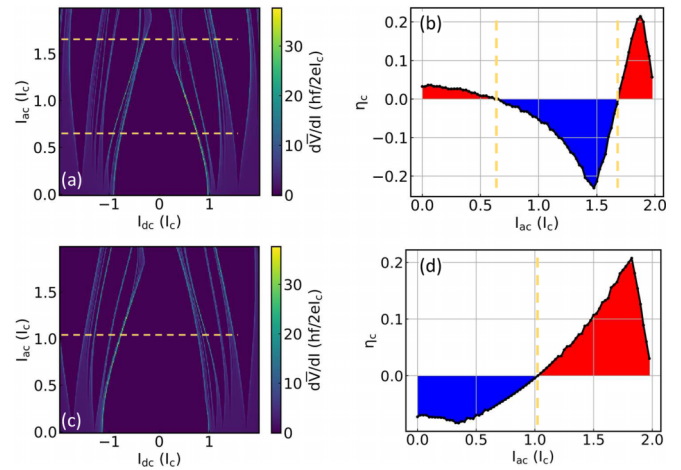

FIG. 4. SQUID microwave response under current bias with $\hat{\Phi} = 3/4$ and $\beta_L = 1$ for (a), (b) the skewed SQUID with $a_1 = 1$, $a_2 = 0.9 = 1 - c_2$, $R_{21} = 2$ and (c), (d) 2π-4π. Dashed lines indicate powers at which $\eta_c = 0$.

Figure 4(a) shows the power dependence of the dV/dI characteristics for a trivial asymmetric SQUID ($\Phi = \Phi_0/4$) where the diode polarity gradually switches at high powers, as shown in Fig. 4(b). Dashed lines indicate a diode polarity switch. In agreement with Figs. 2(c) and 2(d), η_c has a soft sign switch at low power before switching abruptly as the critical currents are nearly suppressed. Also in agreement with Figs. 2(c) and 2(d), η_c has extrema as the critical currents are suppressed. Figures 4(c) and 4(d) present the microwave response of a 2π-4π SQUID. We note that the polarity of the 2π-4π SQUID is opposite to that of the trivial asymmetric SQUID at zero ac power. η_c has a weak enhancement in magnitude at lower I_{AC} before a gradual sign change at $I_{AC} = I_c$, which is at a higher power than the first polarity switch of the asymmetric SQUID ($I_{AC} \approx 0.6I_c$). Generally, the numerical results indicate good agreement with the analytic calculations. The dV/dI characteristics are generally nonreciprocal, showing different Shapiro steps for positive and negative I_{DC} [75].

IV. CONCLUSIONS

In this paper, we studied the JDE in the dc and ac response of asymmetric SQUIDs, including the effects of inductance and asymmetries in I_c and R_n. We showed that the inductance β_L and the ratio $R_{21} = R_{n,2}/R_{n,1}$ can tune the diode efficiency of an asymmetric dc SQUID. Such results may be applicable to recent experimental demonstrations of gate-tunable diode effects in asymmetric SQUIDs [84,85]. For SQUIDs with a 4π junction, tuning β_L and R_{21} can cause a switching on the diode polarity. We also showed a 2π-4π SQUID has the opposite diode polarity of a trivial SQUID over a wide range of $\beta_L/(1 + R_{21})$ and $\hat{\Phi}$. We then discussed how the Josephson diode polarity and efficiency of asymmetric SQUIDs can be controlled by microwave irradiation. We presented calculations of the ac response of asymmetric SQUIDs where the diode efficiency and polarity are controlled by the ac power. The advantage of probing nonreciprocal transport in the ac response is that missing Shapiro steps indicative of a fractional Josephson effect have been observed experimentally

[19,66–70], suggesting the ac response of a 2π-4π SQUID can readily be observed regardless of whether the 4π junction is topological or not.

APPENDIX A: 2π-4π SQUID DYNAMICS

We start with the model for a semiclassical description of SQUID dynamics:

$$I_{\text{bias}} = I_1 + I_2, \tag{A1}$$

$$\phi_2 - \phi_1 = \frac{2\pi}{\Phi_0} \Phi_{\text{tot}}, \tag{A2}$$

$$\Phi_{\text{tot}} = L(I_1 - I_2) + \Phi, \tag{A3}$$

$$I_i = \frac{V_{J,i}}{R} + I_{s,i} + C_i \frac{dV_{J,i}}{dt} \tag{A4}$$

where I_1 and I_2 are the currents in each of the SQUID arms, ϕ_1 and ϕ_2 are the gauge-invariant phase differences across the JJs in each of the SQUID arms, Φ is the total external magnetic flux through the SQUID, L is the inductance associated with the screening flux, and $V_{J,i}$ and $I_{s,i}$ for $i = 1, 2$ are the potential differences across the ith JJ and the pair current in the ith JJ, respectively. We can consider the general resistively and capacitively-shunted junction (RCSJ) model for a SQUID device:

$$\frac{d^2\phi_1}{d\tau'^2} + \sigma \frac{d\phi_1}{d\tau'}$$
$$= \frac{i_B}{2} - i_{s,1}(\phi_1) + \frac{1}{4\pi\beta_L}(\phi_2 - \phi_1 - 2\pi\hat{\Phi}), \tag{A5a}$$

$$C_{21}\frac{d^2\phi_2}{d\tau'^2} + \frac{\sigma}{R_{21}}\frac{d\phi_2}{d\tau'}$$
$$= \frac{i_B}{2} - I_{21}i_{s,2}(\phi_2) - \frac{1}{4\pi\beta_L}(\phi_2 - \phi_1 - 2\pi\hat{\Phi}) \tag{A5b}$$

where $C_{21} = C_2/C_1$, $I_{21} = I_{c,2}/I_{c,1}$, $R_{21} = R_{n,2}/R_{n,1}$, $\sigma = \sqrt{\Phi_0/2\pi I_{c,1}R_{n,1}^2 C_1}$, and $\tau' = \sqrt{2\pi I_{c,1}/\Phi_0 C_1}t$. We will work in the overdamped regime for simplicity, but the extension is straightforward. Numerical calculations are generated by solving the system of coupled differential equations in the overdamped regime where capacitance is neglected.

For a 2π-4π SQUID, we consider the supercurrents $i_{s,1} = \sin(\phi_1)$ and $i_{s,2} = \sin(\phi_2/2)$ where $R_{21} = I_{21} = 1$. We can reduce the SQUID dynamical equations to a single dynamical

equation as a function of the average phase across the SQUID $\phi_A = (\phi_1 + \phi_2)/2$ by considering the inductance β_L to be perturbatively small [80]. The resulting dynamical equation is $i_B/2 = \frac{d\phi_A}{d\tau} + \tilde{i}_s(\phi_A, \hat{\Phi}_{\text{ext}})$ where $\tau \equiv (2\pi R I_{2\pi}/\Phi_0)t$ and

$$\tilde{i}_s(\phi_A, \hat{\Phi}) = \frac{1}{2}\sin\left(\frac{\phi_A + \pi\hat{\Phi}}{2}\right) + \frac{1}{2}\sin\left(\phi_A - \pi\hat{\Phi}\right)$$
$$- \frac{\pi\beta_L}{8}\{2\sin[2(\phi_A - \pi\hat{\Phi})] + \sin(\phi_A + \pi\hat{\Phi})\}$$
$$- \frac{\pi\beta_L}{8}\left[\sin\left(\frac{\phi_A - 3\pi\hat{\Phi}}{2}\right)\right.$$
$$\left. - 3\sin\left(\frac{3\phi_A - \pi\hat{\Phi}}{2}\right)\right]. \tag{A6}$$

DC response

We find that the SQUID dc response to magnetic flux in the 2π-4π SQUID is asymmetric: $I_{\max}(\hat{\Phi}, I_{\text{DC}}) \neq I_{\max}(-\hat{\Phi}, I_{\text{DC}}) \neq I_{\max}(\hat{\Phi}, -I_{\text{DC}})$. The symmetry retained in the system is $I_{\max}(\hat{\Phi}, I_{\text{DC}}) = I_{\max}(-\hat{\Phi}, -I_{\text{DC}})$.

Besides this general asymmetry, we also notice that the maximum critical current does not manifest at $\Phi = 0$. Recall that for a trivial SQUID with sinusoidal CPRs the currents are maximized at $\phi_{\max} = \pi/2$ and the two arms of the SQUID can simultaneously have that phase $\phi_{\max}$ if the magnetic flux is an integer multiple of the magnetic flux quantum:

$$\phi_2 - \phi_1 = \frac{2\pi\Phi}{\Phi_0}(\text{mod }2\pi). \tag{A7}$$

Now, for the 2π-4π SQUID, if the trivial arm (say, arm 1) has $\phi_{\max,1} = \pi/2$ and the nontrivial arm has $\phi_{\max,2} = \pi$, then it follows from the argument for the trivial SQUID that the maximum should occur at $\Phi = \Phi_0/4$.

APPENDIX B: SYMMETRIC SQUID WITH π-, 2π-, AND 4π-PERIODIC CHANNELS

In this section, we provide the general solution for a symmetric dc SQUID circuit model with negligible capacitance, weak inductance, and a supercurrent with π-, 2π-, and 4π-periodic channels. We write an effective description of the supercurrent channel with a skewed CPR and a topological contribution as

$$I_s = I_{4\pi}\sin(\phi/2) + I_{2\pi}\sin(\phi) + I_\pi\sin(2\phi). \tag{B1}$$

Making use of the ac Josephson effect $\frac{d\phi}{dt} = \frac{2e}{\hbar}V$, we find

$$\frac{d\phi_1}{d\tau} + \sin(\phi_1) + \tilde{\beta}\sin(2\phi_1) + \alpha\sin(\phi_1/2) + \frac{\phi_1 - \phi_2}{4\pi\beta_L}$$
$$= \frac{1}{2}\left(i_B - \frac{\hat{\Phi}}{\beta_L}\right), \tag{B2}$$

$$\frac{d\phi_2}{d\tau} + \sin(\phi_2) + \tilde{\beta}\sin(2\phi_2) + \alpha\sin(\phi_2/2) - \frac{\phi_1 - \phi_2}{4\pi\beta_L}$$
$$= \frac{1}{2}\left(i_B + \frac{\hat{\Phi}}{\beta_L}\right) \tag{B3}$$

where $\tilde{\beta} \equiv I_\pi/I_{2\pi}$, $\alpha \equiv I_{4\pi}/I_{2\pi}$, $\beta_L \equiv LI_{2\pi}/\Phi_0$,

$i_B \equiv I_{\text{bias}}/I_{2\pi}$, $\hat{\Phi} \equiv \Phi/\Phi_0$, and $\tau \equiv (2\pi R_{n,1} I_{2\pi}/\Phi_0)t$. Defining $\phi_A \equiv (\phi_1 + \phi_2)/2$ and $\Psi \equiv (\phi_2 - \phi_1)/2\pi$, we can consider the sum and difference of equations to find

$$
\frac{d\phi_A}{d\tau} + \sin(\phi_A)\cos(\pi\Psi) + \tilde{\beta}\sin(2\phi_A)\cos(2\pi\Psi)
$$
$$
+ \alpha\sin(\phi_A/2)\cos(\pi\Psi/2) = \frac{i_B}{2}, \tag{B4}
$$

$$
\pi\frac{d\Psi}{d\tau} + \frac{\Psi}{2\beta_L} + \sin(\pi\Psi)\cos(\Phi_A) + \tilde{\beta}\sin(2\pi\Psi)\cos(2\phi_A)
$$
$$
+ \alpha\sin(\pi\Psi/2)\cos(\phi_A/2) = \frac{\hat{\Phi}}{2\beta_L}. \tag{B5}
$$

Assuming $\beta_L \ll 1$, we make the following ansatz:

$$
\Psi(\tau) = \hat{\Phi} + \beta_L\Psi_1(\tau) + \mathcal{O}(\beta_L^2). \tag{B6}
$$

Substituting, we find the solution to lowest order in β_L is

$$
\Psi_1(\tau) = -2[\alpha\sin(\pi\hat{\Phi}/2)\cos(\phi_A/2)
$$
$$
+ \tilde{\beta}\sin(2\pi\hat{\Phi})\cos(2\phi_A) + \sin(\pi\hat{\Phi})\cos(\phi_A)]. \tag{B7}
$$

Now we can reduce the system of coupled equations into a single equation for ϕ_A and calculate the time-averaged current bias for an rf-driven junction. Substituting Eq. (B7) into Eq. (B4) and simplifying, we find

$$
\frac{d\phi_A}{d\tau} + a\sin(\phi_A) + b\sin(2\phi_A) + c\sin(3\phi_A) + d\sin(4\phi_A)
$$
$$
+ f\sin\left(\frac{\phi_A}{2}\right) + g\sin\left(\frac{3\phi_A}{2}\right) + h\sin\left(\frac{5\phi_A}{2}\right) = \frac{i_B}{2} \tag{B8}
$$

for the coefficients

$$
a = x(1 - \pi\beta_L\tilde{\beta}y^2) + \frac{\pi}{4}\alpha^2\beta_L(1-x), \tag{B9}
$$

$$
b = \tilde{\beta} + (\pi\beta_L - 2\tilde{\beta})y^2, \tag{B10}
$$

$$
c = 6\pi\beta_L\tilde{\beta}xy^2, \tag{B11}
$$

$$
d = 2\pi\beta_L\tilde{\beta}^2y^2, \tag{B12}
$$

$$
f = \alpha\left(C_{\pi/2} + \frac{\pi}{2}\beta_L y S_{\pi/2}\right), \tag{B13}
$$

$$
g = \frac{3\pi}{2}\alpha\beta_L y(1 + 2\tilde{\beta}x)S_{\pi/2}, \tag{B14}
$$

$$
h = 5\pi\alpha\beta_L\tilde{\beta}xy S_{\pi/2} \tag{B15}
$$

where $S_{\pi/2} \equiv \sin(\pi\hat{\Phi}/2)$, $C_{\pi/2} \equiv \cos(\pi\hat{\Phi}/2)$, $x \equiv \cos(\pi\hat{\Phi})$, and $y \equiv \sin(\pi\hat{\Phi})$. Note that if $\hat{\Phi} = 0$ then only a, b, and f are nonzero. The coefficients in Eq. (B8) have the following interpretations: a, the 2π channel of each arm, the *interference* of the 4π channels of the arms, and the interference of the 2π and π channels of the arms; b, the π channel of each arm and the interference of the 2π channels of the arms; c, the interference of the 2π and π channels of the arms; d, the interference of the π channels of the arms; f, the 4π channel of each arm; g, the interference of the 4π and 2π channels of the arms, and the interference of the 4π and π channels of the arms; and h, the interference of the 4π and π channels of the arms.

Voltage-bias solution

From here, we can consider a voltage bias

$$
V(\tau) = V_0 + V_1\cos(\omega\tau) \tag{B16}
$$

and make use of the ac Josephson effect

$$
\frac{d\phi_A}{dt} = \frac{2e}{\hbar}V
$$

to solve for $\phi_A(\tau)$ and substitute into Eq. (B8). Then we can use the Jacobi-Anger expansion,

$$
e^{iz\sin(\theta)} = \sum_{n=-\infty}^{+\infty} J_n(z)e^{in\theta}, \tag{B17}
$$

where J_n are nth-order Bessel functions, to calculate the Shapiro spikes and each spike's width.

Now we will describe how to calculate Shapiro spike widths in terms of the time-averaged pair current $\bar{I}_s$ and specifically consider the $n = 0$ spike. We start by integrating the ac Josephson effect from the end of the previous section. We can write (in dimensionless parameters)

$$
\phi_A(\tau) = \phi_0 + \omega_0\tau + z\sin(\omega\tau) \tag{B18}
$$

where ϕ_0 is an arbitrary integration constant, $z = 2eV_1/\hbar\omega$, and $\omega_0 = 2eV_0/\hbar$. We then substitute into Eq. (B8) to get $2d\phi_A/d\tau + I_s = i_B$ where

$$
I_s = 2\text{Im}\left\{\sum_{n=-\infty}^{+\infty}(-1)^n e^{-in\omega\tau}\left[ae^{i(\phi_0+\omega_0\tau)}J_n(z) + be^{2i(\phi_0+\omega_0\tau)}J_n(2z) + ce^{3i(\phi_0+\omega_0\tau)}J_n(3z)\right.\right.
$$
$$
\left.\left.+ de^{4i(\phi_0+\omega_0\tau)}J_n(4z) + fe^{\frac{1}{2}i(\phi_0+\omega_0\tau)}J_n(z/2) + ge^{\frac{3}{2}i(\phi_0+\omega_0\tau)}J_n(3z/2) + he^{\frac{5}{2}i(\phi_0+\omega_0\tau)}J_n(5z/2)\right]\right\}. \tag{B19}
$$

APPENDIX C: ASYMMETRIC SQUID DYNAMICS

Now we assume a general CPR with π-, 2π-, and 4π-periodic channels:

$$
i_{s,1}(\phi_1) = a_1\sin(\phi_1) + b_1\sin\left(\frac{\phi_1}{2}\right) + c_1\sin(2\phi_1), \tag{C1}
$$

$$
\Delta_{21}i_{s,2}(\phi_2) = a_2\sin(\phi_2) + b_2\sin(\phi/2) + c_2\sin(2\phi_2) \tag{C2}
$$

where $\Delta_{21} = I_{c,2}R_{n,2}/I_{c,1}R_{n,1}$. If we assume β_L, $|1 - R_{21}| \ll 1$ then we can reduce the system of two ordinary differential equations (ODEs) to a single ODE via a perturbative ansatz similar to the ansatz made by de Luca:

$$
\frac{d\phi_A}{d\tau} = \frac{i_B}{2} - \tilde{i}_s(\phi_A) + \frac{\pi\beta_L(c_1 - c_2)^2}{2(1 + R_{21})}S_4 \tag{C3}
$$

where

$$\tilde{i}_s(\phi_A) = x_2 \sin(\phi_A) + x_4 \sin(2\phi_A) + x_6 \sin(3\phi_A) + x_8 \sin(4\phi_A) + x_1 \sin(\phi_A/2) + x_3 \sin(3\phi_A/2) + x_5 \sin(5\phi_A/2)$$

$$+ y_2 \cos(\phi_A) + y_4 \cos(2\phi_A) + y_6 \cos(3\phi_A) + y_8 \cos(4\phi_A) + y_1 \cos(\phi_A/2) + y_3 \cos(3\phi_A/2) + y_5 \cos(5\phi_A/2). \quad \text{(C4)}$$

The coefficients of the effective supercurrent $\tilde{i}_s$ are [$C_n \equiv \cos(n\pi\hat{\Phi})$ and $S_n \equiv \sin(n\pi\hat{\Phi})$]

$$x_2 = \frac{\pi\beta_L b_1 b_2}{2(1+R_{21})} + \left[\frac{a_1+a_2}{2} - \frac{\pi\beta_L}{1+R_{21}}\left(\frac{b_1^2}{2} - a_1 c_1 + a_1 c_2 + \frac{b_2^2}{4} - \frac{a_2 c_1}{2}\right)\right] C_1 - \frac{\pi\beta_L}{1+R_{21}}\left(a_2 c_1 - \frac{a_2 c_2}{2} + \frac{a_1 c_1}{2}\right) C_3, \quad \text{(C5)}$$

$$y_2 = \left[\frac{a_2-a_1}{2} - \frac{\pi\beta_L}{1+R_{21}}\left(a_1 c_1 - \frac{a_1 c_2}{2} + \frac{b_2^2}{4} - \frac{a_2 c_1}{2}\right)\right] S_1 - \frac{\pi\beta_L}{1+R_{21}}\left(\frac{a_2 c_2}{2} - a_2 c_1 + \frac{a_1 c_1}{2}\right) S_3, \quad \text{(C6)}$$

$$x_4 = \frac{\pi\beta_L a_1 a_2}{1+R_{21}} + \left(\frac{c_1+c_2}{2} - \frac{\pi\beta_L(a_1^2+a_2^2)}{2(1+R_{21})}\right) C_2, \quad \text{(C7)}$$

$$y_4 = \left(\frac{c_2-c_1}{2} - \frac{\pi\beta_L(a_2^2-a_1^2)}{4(1+R_{21})}\right) S_2, \quad \text{(C8)}$$

$$x_6 = -\frac{\pi\beta_L}{1+R_{21}}\left(\frac{a_2 c_2}{2} - 2a_2 c_1 - \frac{a_1 c_1}{2} - a_1 c_2\right) C_1 - \frac{\pi\beta_L}{1+R_{21}}\left(2a_1 c_1 + \frac{a_2 c_1}{2} + a_2 c_2 + \frac{a_1 c_2}{2}\right) C_3, \quad \text{(C9)}$$

$$y_6 = -\frac{\pi\beta_L}{1+R_{21}}\left(2a_2 c_1 - \frac{a_2 c_2 + a_1 c_1}{2} - a_1 c_2\right) S_1 - \frac{\pi\beta_L}{1+R_{21}}\left(-2a_1 c_1 + \frac{a_2 c_1}{2} + a_2 c_2 + \frac{a_1 c_2}{2}\right) S_3, \quad \text{(C10)}$$

$$x_8 = -\frac{\pi\beta_L}{1+R_{21}}\left(\frac{c_2^2-c_1^2}{2} - 2c_1 c_2\right) - \frac{\pi\beta_L}{1+R_{21}}\left(\frac{3c_1^2+c_2^2}{2}\right) C_4, \quad \text{(C11)}$$

$$y_8 = -\frac{\pi\beta_L}{1+R_{21}}\left(\frac{-3c_1^2+2c_1 c_2+c_2^2}{2}\right) S_4, \quad \text{(C12)}$$

$$x_1 = \left(\frac{b_1+b_2}{2} + \frac{\pi\beta_L}{1+R_{21}}\frac{a_1 b_1 + a_2 b_2}{4}\right) C_{1/2} - \frac{\pi\beta_L}{1+R_{21}}\left(\frac{a_1 b_2 + a_2 b_1}{4}\right) C_{3/2}, \quad \text{(C13)}$$

$$y_1 = \left(\frac{b_2-b_1}{2} + \frac{\pi\beta_L}{1+R_{21}}\frac{a_2 b_2 - a_1 b_1}{4}\right) S_{1/2} - \frac{\pi\beta_L}{1+R_{21}}\left(\frac{a_2 b_1 - a_1 b_2}{4}\right) S_{3/2}, \quad \text{(C14)}$$

$$x_3 = \frac{\pi\beta_L}{1+R_{21}}\left[\left(\frac{3a_1 b_2 + 3a_2 b_1}{4}\right) C_{1/2} - \left(\frac{3a_1 b_1 - 5b_1 c_1 + 2b_1 c_2 + 3a_2 b_2 - 2b_2 c_1 - b_2 c_2}{4}\right) C_{3/2}\right.$$

$$\left. -\left(\frac{-2b_2 c_2 + 2b_1 c_1 + b_1 c_2 + 5b_2 c_1}{4}\right) C_{5/2}\right], \quad \text{(C15)}$$

$$y_3 = -\frac{\pi\beta_L}{1+R_{21}}\left[\left(\frac{3(a_1 b_2 - a_2 b_1)}{4}\right) S_{1/2} + \left(\frac{-3a_1 b_1 + 5b_1 c_1 - 2b_1 c_2 + 3a_2 b_2 - 2b_2 c_1 - b_2 c_2}{4}\right) S_{3/2}\right.$$

$$\left. +\left(\frac{2b_2 c_2 + 2b_1 c_1 + b_1 c_2 - 5b_2 c_1}{4}\right) S_{5/2}\right], \quad \text{(C16)}$$

$$x_5 = -\frac{\pi\beta_L}{1+R_{21}}\left[\left(\frac{-7b_2 c_1 + 2b_2 c_2 - 2b_1 c_1 - 3b_1 c_2}{4}\right) C_{3/2} + \left(\frac{7b_1 c_1 - 2b_1 c_2 + 2b_2 c_1 + 3b_2 c_2}{4}\right) C_{5/2}\right], \quad \text{(C17)}$$

$$y_5 = -\frac{\pi\beta_L}{1+R_{21}}\left[\left(\frac{7b_2 c_1 - 2b_2 c_2 - 2b_1 c_1 - 3b_1 c_2}{4}\right) S_{3/2} + \left(\frac{-7b_1 c_1 + 2b_1 c_2 + 2b_2 c_1 + 3b_2 c_2}{4}\right) S_{5/2}\right]. \quad \text{(C18)}$$

These are complicated expressions, but we can gain insight about the effects of asymmetry on the dc and ac response of the SQUID. First, we notice that the harmonics entering the effective supercurrent are the same as those in the symmetric
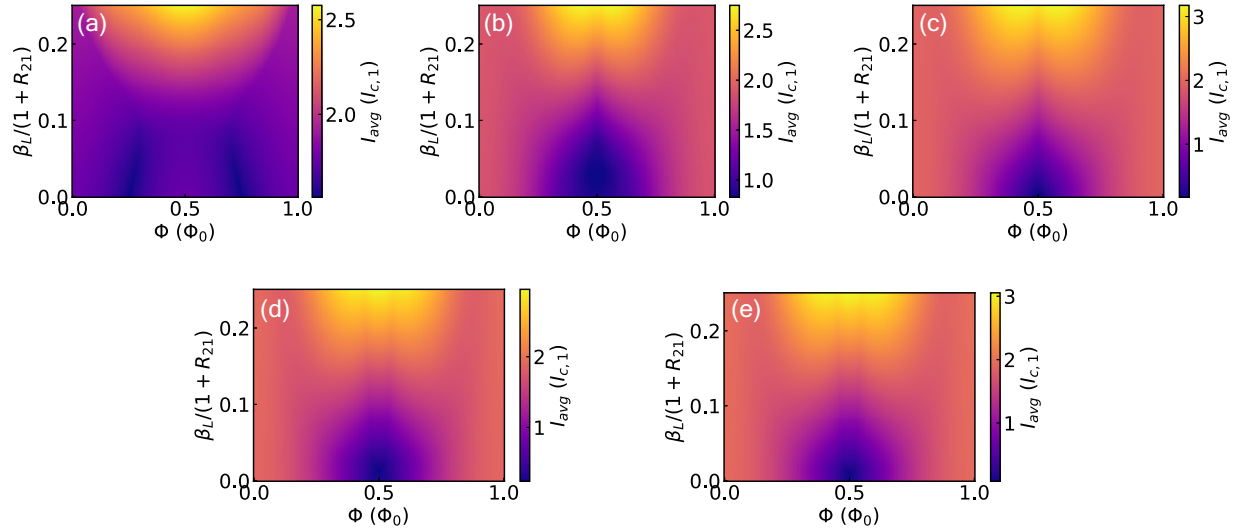
FIG. 5. I_{avg} dependence on Φ and $\frac{\beta_L}{1+R_{21}}$ for $a_1 = 1$ and (a)–(c) various values of $W_{4\pi}$, (e) $a_2 = 0.8$, $b_2 = 0.1 = c_2$, and (f) $a_2 = 0.9 = 1 - c_2$ (trivial SQUID).

case, except here we have both cosine and sine terms. For $\hat{\Phi} = 0$, we have $y_1 = \ldots = y_8 = 0$ so that only the sine terms contribute to the zero-field SQUID response. Interestingly, higher harmonics, e.g., $\sin(2\phi_A)$, contribute to the effective supercurrent at zero field as opposed to the symmetric case where higher harmonic contributions only affect the SQUID response at nonzero magnetic flux.

Voltage-bias solution

As before, we can consider a voltage bias

$$V(\tau) = V_0 + V_1 \cos(\omega\tau) \tag{C19}$$

and make use of the ac Josephson effect

$$\frac{d\phi_A}{dt} = \frac{2e}{\hbar} V \tag{C20}$$

to solve for $\phi_A(\tau)$. Then we can use the Jacobi-Anger expansion,

$$e^{iz\sin(\theta)} = \sum_{n=-\infty}^{+\infty} J_n(z) e^{in\theta}, \tag{C21}$$

where J_n are nth-order Bessel functions, to calculate the Shapiro steps and each step's width.

We can integrate to solve for $\phi_A(\tau)$:

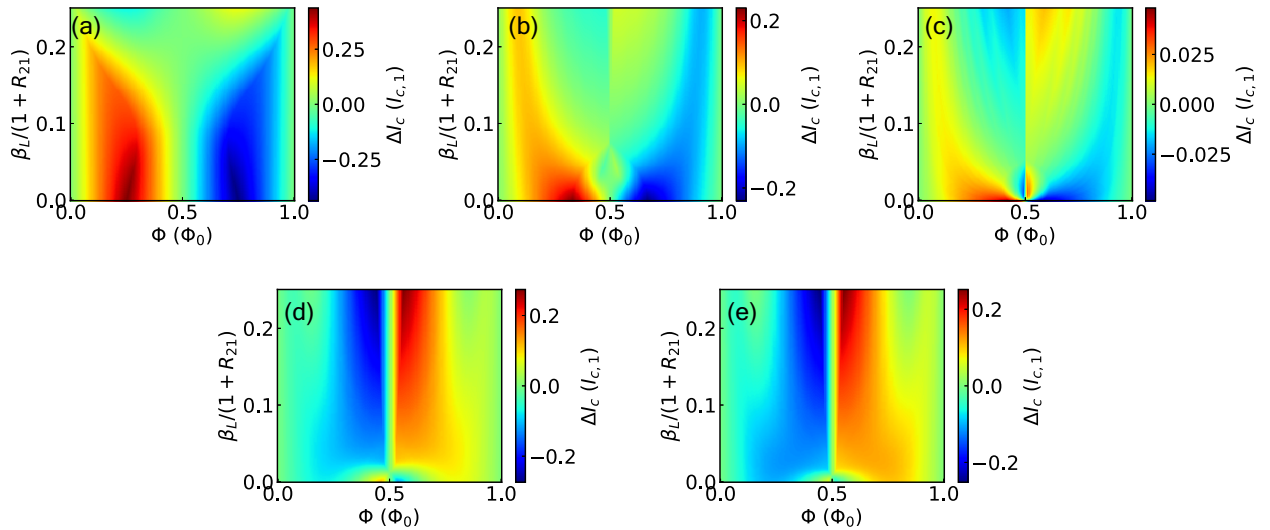$$\phi_A(\tau) = \phi_0 + \omega_0\tau + z\sin(\omega\tau) \tag{C22}$$

FIG. 6. ΔI_c dependence on Φ and $\frac{\beta_L}{1+R_{21}}$ for $a_1 = 1$ and (a)–(c) various values of $W_{4\pi}$, (e) $a_2 = 0.8$, $b_2 = 0.1 = c_2$, and (f) $a_2 = 0.9 = 1 - c_2$ (trivial SQUID).
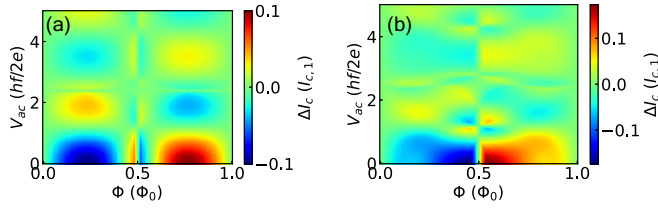
FIG. 7. AC power dependence of ΔI_c for a trivial SQUID with (a) $\frac{\beta_L}{1+R_{21}} = 0$ and (b) $\frac{\beta_L}{1+R_{21}} = 0.125$.
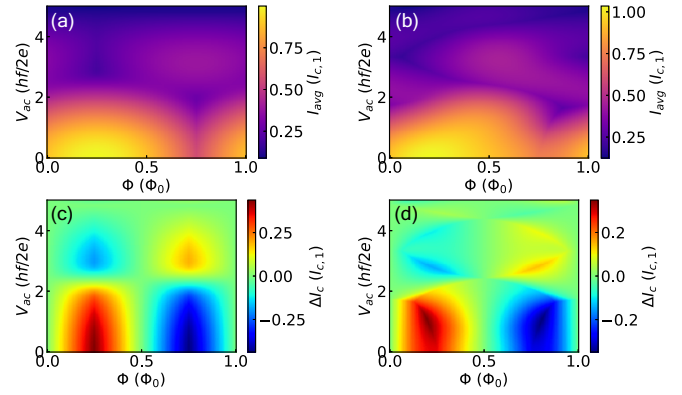

FIG. 8. AC power dependence of I_{avg} and ΔI_c for a 2π-4π SQUID with (a) $\frac{\beta_L}{1+R_{21}} = 0$ and (b) $\frac{\beta_L}{1+R_{21}} = 0.125$.

where ϕ_0 is an arbitrary integration constant, $z = 2eV_1/\hbar\omega$, and $\omega_0 = 2eV_0/\hbar$. Then we have

$$
\begin{aligned}
\bar{I}_s(\phi_0, \omega_0 = m\omega) = \sum_n (-1)^n [&x_2 \sin(\phi_0) J_n(z)\delta_{m,n} + x_4 \sin(2\phi_0) J_n(2z)\delta_{2m,n} \\
&+ x_6 \sin(3\phi_0) J_n(3z)\delta_{3m,n} + x_8 \sin(4\phi_0) J_n(4z)\delta_{4m,n} + x_1 \sin(\phi_0/2) J_n(z/2)\delta_{m/2,n} \\
&+ x_3 \sin(3\phi_0/2) J_n(3z/2)\delta_{3m/2,n} + x_5 \sin(5\phi_0/2) J_n(5z/2)\delta_{5m/2,n} + y_2 \cos(\phi_0) J_n(z)\delta_{m,n} \\
&+ y_4 \cos(2\phi_0) J_n(2z)\delta_{2m,n} + y_6 \cos(3\phi_0) J_n(3z)\delta_{3m,n} + y_8 \cos(4\phi_0) J_n(4z)\delta_{4m,n} \\
&+ y_1 \cos(\phi_0/2) J_n(z/2)\delta_{m/2,n} + y_3 \cos(3\phi_0/2) J_n(3z/2)\delta_{3m/2,n} \\
&+ y_5 \cos(5\phi_0/2) J_n(5z/2)\delta_{5m/2,n}].
\end{aligned}
\tag{C23}
$$

APPENDIX D: ADDITIONAL DATA

Figures 5 and 6 show calculations of the average critical current and critical current difference corresponding to data in Figs. 1(d)–1(h). Figures 7 and 8 show the critical current difference corresponding to data in Figs. 3 and 4, respectively.

[1] M. A. Silaev, A. Y. Aladyshkin, M. V. Silaeva, and A. S. Aladyshkina, The diode effect induced by domain-wall superconductivity, J. Phys.: Condens. Matter **26**, 095702 (2014).

[2] R. Wakatsuki, Y. Saito, S. Hoshino, Y. M. Itahashi, T. Ideue, M. Ezawa, Y. Iwasa, and N. Nagaosa, Nonreciprocal charge transport in noncentrosymmetric superconductors, Sci. Adv. **3**, e1602390 (2017).

[3] K. Yasuda, H. Yasuda, T. Liang, R. Yoshimi, A. Tsukazaki, K. S. Takahashi, N. Nagaosa, M. Kawasaki, and Y. Tokura, Nonreciprocal charge transport at topological insulator/superconductor interface, Nat. Commun. **10**, 2734 (2019).

[4] F. Ando, Y. Miyasaka, T. Li, J. Ishizuka, T. Arakawa, Y. Shiota, T. Moriyama, Y. Yanase, and T. Ono, Observation of superconducting diode effect, Nature (London) **584**, 373 (2020).

[5] J. Shin, S. Son, J. Yun, G. Park, K. Zhang, Y. J. Shin, J.-G. Park, and D. Kim, Magnetic proximity-induced superconducting diode effect and infinite magnetoresistance in van der Waals heterostructure, Phys. Rev. Res. **5**, 043029 (2023).

[6] Y.-Y. Lyu, J. Jiang, Y.-L. Wang, Z.-L. Xiao, S. Dong, Q.-H. Chen, M. V. Milošević, H. Wang, R. Divan, J. E. Pearson, P. Wu, F. M. Peeters, and W.-K. Kwok, Superconducting diode effect via conformal-mapped nanoholes, Nat. Commun. **12**, 2703 (2021).

[7] A. Daido, Y. Ikeda, and Y. Yanase, Intrinsic superconducting diode effect, Phys. Rev. Lett. **128**, 037001 (2022).

[8] N. F. Q. Yuan and L. Fu, Supercurrent diode effect and finite-momentum superconductors, Proc. Natl. Acad. Sci. USA **119**, e2119548119 (2022).

[9] S. Ilić and F. S. Bergeret, Theory of the supercurrent diode effect in Rashba superconductors with arbitrary disorder, Phys. Rev. Lett. **128**, 177001 (2022).

[10] H. F. Legg, D. Loss, and J. Klinovaja, Superconducting diode effect due to magnetochiral anisotropy in topological insulators and Rashba nanowires, Phys. Rev. B **106**, 104501 (2022).

[11] D. Suri, A. Kamra, T. N. G. Meier, M. Kronseder, W. Belzig, C. H. Back, and C. Strunk, Non-reciprocity of vortex-limited

critical current in conventional superconducting micro-bridges, Appl. Phys. Lett. **121**, 102601 (2022).

[12] J. J. He, Y. Tanaka, and N. Nagaosa, A phenomenological theory of superconductor diodes, New J. Phys. **24**, 053014 (2022).

[13] T. Karabassov, I. V. Bobkova, A. A. Golubov, and A. S. Vasenko, Hybrid helical state and superconducting diode effect in superconductor/ferromagnet/topological insulator heterostructures, Phys. Rev. B **106**, 224509 (2022).

[14] L. Bauriedl, C. Bäuml, L. Fuchs, C. Baumgartner, N. Paulik, J. M. Bauer, K.-Q. Lin, J. M. Lupton, T. Taniguchi, K. Watanabe, C. Strunk, and N. Paradiso, Supercurrent diode effect and magnetochiral anisotropy in few-layer NbSe2, Nat. Commun. **13**, 4266 (2022).

[15] E. Strambini, M. Spies, N. Ligato, S. Ilifć, M. Rouco, C. Gonzalez-Orellana, M. Ilyn, C. Rogero, F. S. Bergeret, J. S. Moodera, P. Virtanen, T. T. Heikkila, and F. Giazotto, Superconducting spintronic tunnel diode, Nat. Commun. **13**, 2431 (2022).

[16] S. Chahid, S. Teknowijoyo, I. Mowgood, and A. Gulian, High-frequency diode effect in superconducting Nb3Sn microbridges, Phys. Rev. B **107**, 054506 (2023).

[17] J. Hu, C. Wu, and X. Dai, Proposed design of a Josephson diode, Phys. Rev. Lett. **99**, 067004 (2007).

[18] X. Shi, W. Yu, Z. Jiang, B. Andrei Bernevig, W. Pan, S. D. Hawkins, and J. F. Klem, Giant supercurrent states in a superconductor-InAs/GaSb-superconductor junction, J. Appl. Phys. **118**, 133905 (2015).

[19] E. Bocquillon, R. S. Deacon, J. Wiedenmann, P. Leubner, T. M. Klapwijk, C. Brüne, K. Ishibashi, H. Buhmann, and L. W. Molenkamp, Gapless Andreev bound states in the quantum spin Hall insulator HgTe, Nat. Nanotechnol. **12**, 137 (2017).

[20] S. Pal and C. Benjamin, Quantized Josephson phase battery, Europhys. Lett. **126**, 57002 (2019).

[21] K. Misaki and N. Nagaosa, Theory of the nonreciprocal Josephson effect, Phys. Rev. B **103**, 245302 (2021).

[22] C. Baumgartner, L. Fuchs, A. Costa, J. Picó-Cortés, S. Reinhardt, S. Gronin, G. C. Gardner, T. Lindemann, M. J. Manfra, P. E. F. Junior, D. Kochan, J. Fabian, N. Paradiso, and C. Strunk, Effect of Rashba and Dresselhaus spin-orbit coupling on supercurrent rectification and magnetochiral anisotropy of ballistic Josephson junctions, J. Phys.: Condens. Matter **34**, 154005 (2022).

[23] C. Baumgartner, L. Fuchs, A. Costa, S. Reinhardt, S. Gronin, G. C. Gardner, T. Lindemann, M. J. Manfra, P. E. Faria Junior, D. Kochan, J. Fabian, N. Paradiso, and C. Strunk, Supercurrent rectification and magnetochiral effects in symmetric Josephson junctions, Nat. Nanotechnol. **17**, 39 (2022).

[24] K.-R. Jeon, J.-K. Kim, J. Yoon, J.-C. Jeon, H. Han, A. Cottet, T. Kontos, and S. S. P. Parkin, Zero-field polarity-reversible Josephson supercurrent diodes enabled by a proximity-magnetized Pt barrier, Nat. Mater. **21**, 1008 (2022).

[25] K. Halterman, M. Alidoust, R. Smith, and S. Starr, Supercurrent diode effect, spin torques, and robust zero-energy peak in planar half-metallic trilayers, Phys. Rev. B **105**, 104508 (2022).

[26] B. Pal, A. Chakraborty, P. K. Sivakumar, M. Davydova, A. K. Gopi, A. K. Pandeya, J. A. Krieger, Y. Zhang, M. Date, S. Ju, N. Yuan, N. B. M. Schröter, L. Fu, and S. S. P. Parkin, Josephson diode effect from cooper pair momentum in a topological semimetal, Nat. Phys. **18**, 1228 (2022).

[27] H. Wu, Y. Wang, Y. Xu, P. K. Sivakumar, C. Pasco, U. Filippozzi, S. S. P. Parkin, Y.-J. Zeng, T. McQueen, and M. N. Ali, The field-free Josephson diode in a van der Waals heterostructure, Nature (London) **604**, 653 (2022).

[28] T. H. Kokkeler, A. A. Golubov, and F. S. Bergeret, Field-free anomalous junction and superconducting diode effect in spin-split superconductor/topological insulator junctions, Phys. Rev. B **106**, 214504 (2022).

[29] Y. Zhang, Y. Gu, P. Li, J. Hu, and K. Jiang, General theory of Josephson diodes, Phys. Rev. X **12**, 041013 (2022).

[30] M. Davydova, S. Prembabu, and L. Fu, Universal Josephson diode effect, Sci. Adv. **8**, eabo0309 (2022).

[31] S. Ilić, P. Virtanen, T. T. Heikkilä, and F. S. Bergeret, Current rectification in junctions with spin-split superconductors, Phys. Rev. Appl. **17**, 034049 (2022).

[32] M. Trahms, L. Melischek, J. F. Steiner, B. Mahendru, I. Tamir, N. Bogdanoff, O. Peters, G. Reecht, C. B. Winkelmann, F. von Oppen, and K. J. Franke, Diode effect in Josephson junctions with a single magnetic atom, Nature (London) **615**, 628 (2023).

[33] L. Onsager, Reciprocal relations in irreversible processes, I. Phys. Rev. **37**, 405 (1931).

[34] R. Kubo, Statistical-mechanical theory of irreversible processes, I. General theory and simple applications to magnetic and conduction problems, J. Phys. Soc. Jpn. **12**, 570 (1957).

[35] G. L. J. A. Rikken, J. Fölling, and P. Wyder, Electrical magnetochiral anisotropy, Phys. Rev. Lett. **87**, 236602 (2001).

[36] V. M. Krasnov, V. A. Oboznov, and N. F. Pedersen, Fluxon dynamics in long Josephson junctions in the presence of a temperature gradient or spatial nonuniformity, Phys. Rev. B **55**, 14486 (1997).

[37] N. Touitou, P. Bernstein, J. F. Hamet, Ch. Simon, L. Méchin, J. P. Contour, and E. Jacquet, Nonsymmetric current-voltage characteristics in ferromagnet/superconductor thin film structures, Appl. Phys. Lett. **85**, 1742 (2004).

[38] D. Y. Vodolazov, B. A. Gribkov, S. A. Gusev, A. Yu. Klimov, Yu. N. Nozdrin, V. V. Rogov, and S. N. Vdovichev, Considerable enhancement of the critical current in a superconducting film by a magnetized magnetic strip, Phys. Rev. B **72**, 064509 (2005).

[39] A. Papon, K. Senapati, and Z. H. Barber, Asymmetric critical current of niobium microbridges with ferromagnetic stripe, Appl. Phys. Lett. **93**, 172507 (2008).

[40] G. Carapella, P. Sabatino, and G. Costabile, Asymmetry, bistability, and vortex dynamics in a finite-geometry ferromagnet-superconductor bilayer structure, Phys. Rev. B **81**, 054503 (2010).

[41] T. Golod and V. M. Krasnov, Demonstration of a superconducting diode-with-memory, operational at zero magnetic field with switchable nonreciprocity, Nat. Commun. **13**, 3658 (2022).

[42] A. Yu. Kitaev, Fault-tolerant quantum computation by anyons, Ann. Phys. **303**, 2 (2003).

[43] H.-J. Kwon, K. Sengupta, and V. M. Yakovenko, Fractional ac Josephson effect in *p*- and *d*-wave superconductors, Eur. Phys. J. B **37**, 349 (2004).

[44] C. Nayak, S. H. Simon, A. Stern, M. Freedman, and S. Das Sarma, Non-Abelian anyons and topological quantum computation, Rev. Mod. Phys. **80**, 1083 (2008).

[45] L. Fu and C. L. Kane, Josephson current and noise at a superconductor/quantum-spin-Hall-insulator/superconductor junction, Phys. Rev. B **79**, 161408(R) (2009).

[46] J. D. Sau, R. M. Lutchyn, S. Tewari, and S. Das Sarma, Generic new platform for topological quantum computation using semiconductor heterostructures, Phys. Rev. Lett. **104**, 040502 (2010).

[47] J. Alicea, New directions in the pursuit of Majorana fermions in solid state systems, Rep. Prog. Phys. **75**, 076501 (2012).

[48] F. Pientka, A. Keselman, E. Berg, A. Yacoby, A. Stern, and B. I. Halperin, Topological superconductivity in a planar Josephson junction, Phys. Rev. X **7**, 021032 (2017).

[49] M. Hell, M. Leijnse, and K. Flensberg, Two-dimensional platform for networks of Majorana bound states, Phys. Rev. Lett. **118**, 107701 (2017).

[50] D. Aasen, M. Hell, R. V. Mishmash, A. Higginbotham, J. Danon, M. Leijnse, T. S. Jespersen, J. A. Folk, C. M. Marcus, K. Flensberg, and J. Alicea, Milestones toward Majorana-based quantum computing, Phys. Rev. X **6**, 031016 (2016).

[51] E. J. H. Lee, X. Jiang, R. Aguado, G. Katsaros, C. M. Lieber, and S. De Franceschi, Zero-bias anomaly in a nanowire quantum dot coupled to superconductors, Phys. Rev. Lett. **109**, 186802 (2012).

[52] G. Kells, D. Meidan, and P. W. Brouwer, Near-zero-energy end states in topologically trivial spin-orbit coupled superconducting nanowires with a smooth confinement, Phys. Rev. B **86**, 100503(R) (2012).

[53] J. Cayao, E. Prada, P. San-Jose, and R. Aguado, Sns junctions in nanowires with spin-orbit coupling: Role of confinement and helicity on the subgap spectrum, Phys. Rev. B **91**, 024514 (2015).

[54] C. Reeg, O. Dmytruk, D. Chevallier, D. Loss, and J. Klinovaja, Zero-energy Andreev bound states from quantum dots in proximitized Rashba nanowires, Phys. Rev. B **98**, 245407 (2018).

[55] F. Peñaranda, R. Aguado, P. San-Jose, and E. Prada, Quantifying wave-function overlaps in inhomogeneous Majorana nanowires, Phys. Rev. B **98**, 235406 (2018).

[56] A. Vuik, B. Nijholt, A. R. Akhmerov, and M. Wimmer, Reproducing topological properties with quasi-Majorana states, SciPost Phys. **7**, 061 (2019).

[57] C.-X. Liu, J. D. Sau, T. D. Stanescu, and S. Das Sarma, Conductance smearing and anisotropic suppression of induced superconductivity in a Majorana nanowire, Phys. Rev. B **99**, 024510 (2019).

[58] J. Chen, B. D. Woods, P. Yu, M. Hocevar, D. Car, S. R. Plissard, E. P. A. M. Bakkers, T. D. Stanescu, and S. M. Frolov, Ubiquitous non-Majorana zero-bias conductance peaks in nanowire devices, Phys. Rev. Lett. **123**, 107703 (2019).

[59] O. A. Awoga, J. Cayao, and A. M. Black-Schaffer, Supercurrent detection of topologically trivial zero-energy states in nanowire junctions, Phys. Rev. Lett. **123**, 117001 (2019).

[60] B. D. Woods, J. Chen, S. M. Frolov, and T. D. Stanescu, Zero-energy pinning of topologically trivial bound states in multiband semiconductor-superconductor nanowires, Phys. Rev. B **100**, 125407 (2019).

[61] E. Prada, P. San-Jose, M. W. A. de Moor, A. Geresdi, E. J. H. Lee, J. Klinovaja, D. Loss, J. Nygård, R. Aguado, and L. P. Kouwenhoven, From Andreev to Majorana bound states in hybrid superconductor-semiconductor nanowires, Nat. Rev. Phys. **2**, 575 (2020).

[62] M. Valentini, F. Peñaranda, A. Hofmann, M. Brauns, R. Hauschild, P. Krogstrup, P. San-Jose, E. Prada, R. Aguado, and G. Katsaros, Nontopological zero-bias peaks in full-shell nanowires induced by flux-tunable Andreev states, Science **373**, 82 (2021).

[63] R. Hess, H. F. Legg, D. Loss, and J. Klinovaja, Local and non-local quantum transport due to Andreev bound states in finite Rashba nanowires with superconducting and normal sections, Phys. Rev. B **104**, 075405 (2021).

[64] M. C. Dartiailh, W. Mayer, J. Yuan, K. S. Wickramasinghe, A. Matos-Abiague, I. Žutić, and J. Shabani, Phase signature of topological transition in Josephson junctions, Phys. Rev. Lett. **126**, 036802 (2021).

[65] M. Aghaee et al. (Microsoft Quantum), InAs-Al hybrid devices passing the topological gap protocol, Phys. Rev. B **107**, 245423 (2023).

[66] L. P. Rokhinson, X. Liu, and J. K. Furdyna, The fractional a.c. Josephson effect in a semiconductor-superconductor nanowire as a signature of Majorana particles, Nat. Phys. **8**, 795 (2012).

[67] J. Wiedenmann, E. Bocquillon, R. S. Deacon, S. Hartinger, O. Herrmann, T. M. Klapwijk, L. Maier, C. Ames, C. Brüne, C. Gould, A. Oiwa, K. Ishibashi, S. Tarucha, H. Buhmann, and L. W. Molenkamp, 4φ-periodic Josephson supercurrent in HgTe-based topological Josephson junctions, Nat. Commun. **7**, 10303 (2016).

[68] W. Yu, W. Pan, D. L. Medlin, M. A. Rodriguez, S. R. Lee, Z. Q. Bao, and F. Zhang, π and 4π Josephson effects mediated by a Dirac semimetal, Phys. Rev. Lett. **120**, 177704 (2018).

[69] D.-X. Qu, J. J. Cuozzo, N. E. Teslich, K. G. Ray, Z. Dai, T. T. Li, G. F. Chapline, J. L. DuBois, and E. Rossi, Phase-slip lines and anomalous Josephson effects in a tungsten clusters-topological insulator microbridge, arXiv:2301.00086.

[70] M. C. Dartiailh, J. J. Cuozzo, B. H. Elfeky, W. Mayer, J. Yuan, K. S. Wickramasinghe, E. Rossi, and J. Shabani, Missing Shapiro steps in topologically trivial Josephson junction on InAs quantum well, Nat. Commun. **12**, 78 (2021).

[71] A. A. Kopasov, A. G. Kutlin, and A. S. Mel'nikov, Geometry controlled superconducting diode and anomalous Josephson effect triggered by the topological phase transition in curved proximitized nanowires, Phys. Rev. B **103**, 144520 (2021).

[72] H. F. Legg, K. Laubscher, D. Loss, and J. Klinovaja, Parity protected superconducting diode effect in topological Josephson junctions, arXiv:2301.13740 (2023).

[73] T. A. Fulton, L. N. Dunkleberger, and R. C. Dynes, Quantum interference properties of double Josephson junctions, Phys. Rev. B **6**, 855 (1972).

[74] Ya. V. Fominov and D. S. Mikhailov, Asymmetric higher-harmonic SQUID as a Josephson diode, Phys. Rev. B **106**, 134514 (2022).

[75] R. S. Souto, M. Leijnse, and C. Schrade, Josephson diode effect in supercurrent interferometers, Phys. Rev. Lett. **129**, 267702 (2022).

[76] B. van Heck, F. Hassler, A. R. Akhmerov, and C. W. J. Beenakker, Coulomb stability of the 4π-periodic Josephson effect of Majorana fermions, Phys. Rev. B **84**, 180502 (2011).

[77] R. A. Snyder, C. J. Trimble, C. C. Rong, P. A. Folkes, P. J. Taylor, and J. R. Williams, Weak-link Josephson junctions made from topological crystalline insulators, Phys. Rev. Lett. **121**, 097701 (2018).

[78] G. H. Lee, S. Kim, S. H. Jhi, and H. J. Lee, Ultimately short ballistic vertical graphene Josephson junctions, Nat. Commun. **6**, 6181 (2015).

[79] R. Panghotra, B. Raes, C. C. de Souza Silva, I. Cools, W. Keijers, J. E. Scheerder, V. V. Moshchalkov, and J. Van de Vondel, Giant fractional Shapiro steps in anisotropic Josephson junction arrays, Commun. Phys. **3**, 53 (2020).

[80] F. Romeo and R. De Luca, Shapiro steps in symmetric π-SQUID's, Physica C **421**, 35 (2005).

[81] x_m and y_m are defined explicitly in Appendix C.

[82] M. Veldhorst, C. G. Molenaar, C. J. M. Verwijs, H. Hilgenkamp, and A. Brinkman, Optimizing the Majorana character of SQUIDs with topologically nontrivial barriers, Phys. Rev. B **86**, 024509 (2012).

[83] In terms of physical parameters, we can take $I_{c,1} = 0.5\,\mu$A and $R_{n,1} = 85\Omega$ ($E_{J,1} = 2eI_{c,1}$ and $R_{n,1} = 85\mu$eV) at driving frequencies 2, 7, and 12 GHz.

[84] C. Ciaccia, R. Haller, A. C. C. Drachmann, T. Lindemann, M. J. Manfra, C. Schrade, and C. Schönenberger, Gate-tunable Josephson diode in proximitized inas supercurrent interferometers, Phys. Rev. Res. **5**, 033131 (2023).

[85] A. Leblanc, C. Tangchingchai, Z. S. Momtaz, E. Kiyooka, J.-M. Hartmann, G. T. Fernandez-Bada, B. Brun-Barriere, V. Schmitt, S. Zihlmann, R. Maurand, E. Dumur, S. De Franceschi, and F. Lefloch, From nonreciprocal to charge-4e supercurrents in Ge-based Josephson devices with tunable harmonic content, arXiv:2311.15371.